Indenter Tip Radius and Micro-Indentation Hardness

C.J. Tao, T.C. Wang*, X.Y. Feng and S.H. Chen

LNM, Institute of Mechanics, Chinese Academy of Sciences, Beijing 100080, China;
**E-mail: tcwang@imech.ac.cn*

Abstract. Using finite element method with the conventional J_2 theory and strain gradient theory respectively, the effect of the indenter tip radius on the micro-indentation hardness is investigated in the present paper. It is found that the former can not predict the size effect even considering the indenter tip radius, while the latter gives a good agreement to the experimentally measured micro-indentation hardness, which confirms that the size effect of micro-indentation hardness does exist due to the factor of the strain gradient effect.

Key words: finite element method, size effect, micro-indentation hardness, indenter tip radius, conventional J_2 theory, strain gradient theory.

1 Introduction

When a material or a structure possesses a micrometer scale, some mechanical characters are different totally from those in macro scale. Size effect is a main phenomenon found in the micro-scale, especially for the micro-indentation hardness [1–3]. The micro-indentation hardness increases as the indent depth decreases, which can not be explained by the conventional plasticity theory due to no length scale is included. Strain gradient theories are proposed as an effectively theoretical tool to understand the size effect, see for example [4–8].

Using the strain gradient theories, the size effect in micro-indentation hardness has been studied [9–11] with an assumption that the indenter tip is perfect without a curvature and the theoretically predicted results are consistent well with the experimentally measured data.

As for the size effect in micro-indentation hardness, some researchers thought that many experimental factors, such as the effect of the surface layer, the friction between the indenter and the indented material, the indenter tip curvature, should have a great influence on the measured hardness, which could cause an increasing indentation hardness for a decreasing indent depth [12]. However, recent experiments carried out by Swadener et al. [13] on a fine-grained polycrystalline iridium using spherical indenters with different radius show a different trend from [12]: at a fixed

Yilong Bai et al. (eds), IUTAM Symposium on Mechanical Behavior and Micro-Mechanics of Nanostructured Materials, 191–199.

indenter radius, the hardness decreases with the indentation depth decreasing for the case of $a/R < 0.2$. One question arises from [12] and [13]: which result is right? Of course, experiment is a believable truth, which is always adopted to check the correctness of any theory.

In the present paper, the micro-indentation hardness tests will be analyzed numerically using finite element method with the conventional J_2 theory and strain gradient theory proposed by Chen and Wang [7, 8] respectively. A conical indenter with a round tip is considered. The effect of the indenter tip radius on the micro-indentation hardness is emphasized.

The strain gradient theory is briefly reviewed in Section 2. The finite element analysis in the present paper is given in Section 3. In Section 4, numerical results are compared to the existing experimental data for several materials.

2 Review of Strain Gradient Theory

The incremental constitutive relations of the strain gradient theory [7, 8] are

$$\begin{cases} \dot{\sigma}_{ij} = 2\mu\dot{\varepsilon}'_{ij} + K\dot{\varepsilon}_m\delta_{ij}, \\ \dot{m}_{ij} = 2\mu l_{cs}^2\dot{\chi}'_{ij} + K_1 l_{cs}^2\cdot\chi_m\delta_{ij}, \end{cases} \quad \Sigma_e < \sigma_Y, \tag{1}$$

$$\begin{cases} \dot{\sigma}_{ij} = \dfrac{2\Sigma_e}{3E_e}\dot{\varepsilon}'_{ij} + \dfrac{2\dot{\Sigma}_e}{3E_e}\dot{\varepsilon}_{ij} - \dfrac{2\Sigma_e}{3E_e^2}\dot{\varepsilon}_{ij}\dot{E}_e + K\dot{\varepsilon}_m\delta_{ij}, \\ \dot{m}_{ij} = \dfrac{2\Sigma_e}{3E_e}l_{cs}^2\dot{\chi}'_{ij} + \dfrac{2\dot{\Sigma}_e}{3E_e}l_{cs}^2\dot{\chi}'_{ij} - \dfrac{2\Sigma_e}{3E_e^2}l_{cs}^2\chi'_{ij}\dot{E}_e + K_1 l_{cs}^2\dot{\chi}_m\delta_{ij}, \end{cases} \quad \Sigma_e \geq \sigma_Y, \tag{2}$$

where the generalized effective strain and the generalized effective stress are defined as

$$\begin{cases} E_e^2 = \varepsilon_e^2 + l_{cs}^2\chi_e^2,\ \Sigma_e = (\sigma_e^2 + l_{cs}^{-2}m_e^2)^{1/2}, \\ \sigma_e^2 = \dfrac{3}{2}s_{ij}s_{ij}, \qquad m_e^2 = \dfrac{3}{2}m'_{ij}m'_{ij}. \end{cases} \tag{3}$$

Here ε_e is the effective strain, χ_e the effective rotation gradient and η_1 the effective stretch gradient, defined by Fleck and Hutchinson [4].

$$\varepsilon_e = \sqrt{\frac{2}{3}\varepsilon'_{ij}\varepsilon'_{ij}}, \quad \chi_e = \sqrt{\frac{3}{2}\chi_{ij}\chi_{ij}}, \quad \eta_1 = \sqrt{\eta^{(1)}_{ijk}\eta^{(1)}_{ijk}}. \tag{4}$$

The rotation gradient χ_{ij} is defined as a curvature tensor related to the micro-rotation ω_i,

$$\chi_{ij} = \omega_{i,j}. \tag{5}$$

l_{cs} is an intrinsic material length scale required on dimensional grounds. K is the volumetric modulus, K_1 the bend-torsion volumetric modulus. The influence of stretch gradient is introduced by the following hardening law,

$$\begin{cases} \dot{\Sigma}_e = A'(E_e)\left(1+\dfrac{l_1\eta_1}{E_e}\right)^{1/2}\dot{E}_e = B(E_e, l_1\eta_1)\dot{E}_e, & \Sigma_e \geq \sigma_Y, \\ \dot{\Sigma}_e = 3\mu\dot{E}_e, & \Sigma_e < \sigma_Y, \end{cases} \tag{6}$$

where $B(E_e, l_1\eta_1)$ is the hardening function; σ_Y is the yield stress and μ is the shear modulus; For power law hardening material, $A(E_e) = \sigma_Y E_e^n$; l_1 is the second intrinsic material length associated with the stretch gradient. The strain gradient theory [7, 8] reduces to the conventional J_2 deformation theory in the absence of strain gradient effects.

3 Finite Element Analysis

The principal of virtual work and the detailed formulas of the finite element method for the strain gradient theory [7, 8] can be found in [10].

3.1 The Coordinate System

It is convenient to express the field quantities in terms of cylindrical coordinate system (r, θ, z). Both the geometry of the indented solid and loading are axis-symmetric. The displacement field of the indented solid is

$$u_r = u_r(r, z), \quad u_\theta = 0, \quad u_z = u_z(r, z) \tag{7}$$

and the micro-rotation field is

$$\omega_\theta = \omega_\theta(r, z), \quad \omega_r = \omega_z = 0. \tag{8}$$

3.2 The Blunt Conical Indenter

In order to simulate the micro-indentation test, the axis-symmetric model is adopted in this paper. The blunt conical indenter and the axis-symmetric model are shown in Figure 1. The contact depth can be expressed as:

$$\begin{cases} \delta(r) = \dfrac{r}{\tan\beta} - \xi, & r_0 \leq r \leq a, \\ \delta(r) = R - (R^2 - r^2)^{1/2}, & r \leq r_0, \end{cases} \tag{9}$$

where $r_0 = R\cos\beta$, $\xi = R/\sin\beta - R$.

The assumptions in the numerical simulations and the boundary conditions can be found in [10]. The indented body is taken to be a circular cylinder. The size of the indented body is much larger than the depth of the indentation. On the whole surface of the cylinder, the torque tractions are taken to be zero, which yields $\omega_i = 0$, $m_{ij} = 0$ so that the influence of l_{cs} can be ignored.

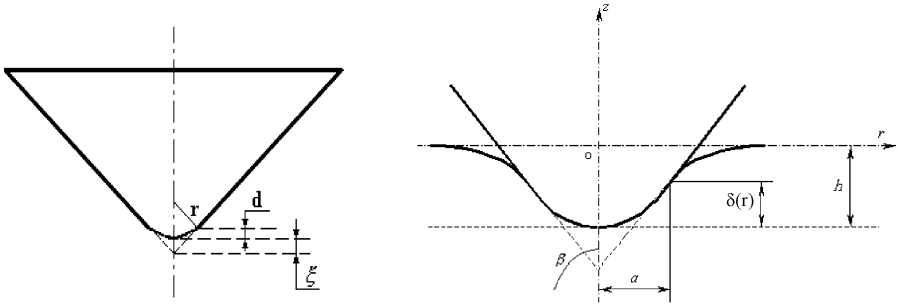

a. Blunt conical indenter $(R \neq 0)$ b. Axis-symmetric indentation model

Fig. 1. Blunted conical indenter and axis-symmetric model.

3.3 The Material Parameters

Young's modulus and Poisson ratio can be obtained from the existing literature – but the yield stress, power-law hardening exponent and intrinsic length scale need to be determined by the numerical fitting method based on the simulation for the experiment data. Following is the detailed steps:

1. Choose three values of depths h_0, h_1, h_2 at large depth where the indentation hardness nearly keeps constant, the corresponding loads $P(h_0)$, $P(h_1)$, $P(h_2)$ can be obtained from the experiment data.
2. First, the values of n and l_1 are prescribed and the initial value σ_Y is chosen as $\sigma_y = \sigma$, one can get $P^*(h_0, \sigma, n, l_1)$, $P^*(h_1, \sigma, n, l_1)$ and $P^*(h_2, \sigma, n, l_1)$ by finite element calculations.
3. Introducing

$$F(\sigma, n, l_1) = \sum_{i=0}^{2} (P^*(h_i, \sigma, n, l_1) - P(h_i))^2,$$

one can get the proper σ^* by the quasi-Newton method [14]:

$$\sigma_{k+1} = \sigma_k - \frac{F(\sigma_k)}{F'(\sigma_k)}, \quad F'(\sigma_k) = \frac{F(\sigma_k) - F(\sigma_{k-1})}{\sigma_k - \sigma_{k-1}},$$

which makes the functional F to be minimum $\min_\sigma F(\sigma, n, l_1) = G(n, l_1)$. Obviously, σ^* depends on n and l_1 , that is, $\sigma^* = \sigma^*(n, l_1)$.

4. Keeping l_1 as a constant, for a given value n $(0 \leq n \leq 1)$, carrying out the above calculations to get each $G(n, l_1)$, then from the curve $G(n, l_1)$ versus n, one can get the proper value n^*, which makes the functional G to be minimum $T(l_1) = \min_n G(n, l_1) = G(n^*, l_1)$.
5. Finally, for a given value l_1 $(0 < l_1 < 1\ \mu\text{m})$, carrying out above calculations to get each $T(l_1)$, then from the curve $T(l_1)$ versus l_1 to make $\min_{l_1} T(l_1) = T(l_1^*)$. The final parameters σ^n, n^* and l_1^* are the needed yield stress σ_Y, the power-law hardening exponent n and the intrinsic length scales l_1.

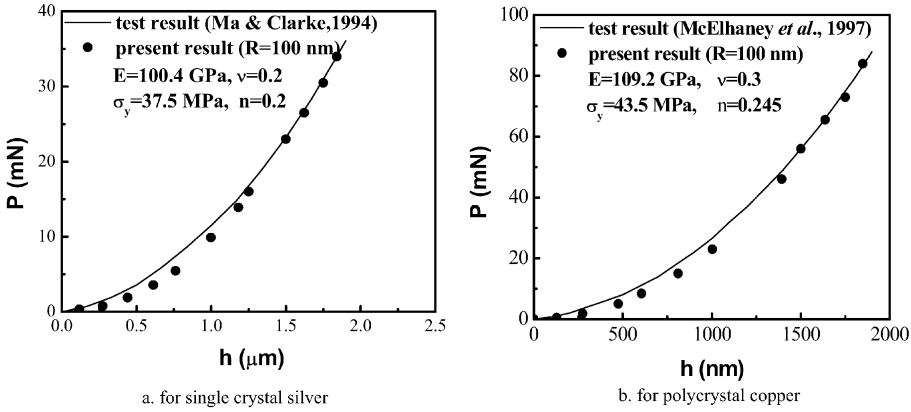

a. for single crystal silver

b. for polycrystal copper

Fig. 2. The indentation load P versus depth h, the calculation results are based on the classical J_2 plasticity theory.

4 Calculation Results and Comparison with the Test Data

The calculation results are shown in this section. Comparisons between the calculation results and the experimental indentation data are emphasized. The indenter tip radius is taken to be $R = 100$ nm.

4.1 Calculation Results and Comparison with the Test Data

Figure 2a shows the results of the indentation load P versus indentation depth h for single crystal silver. The solid line is the experimental results given by Ma and Clarke [2] and the full circles are the present calculation results. Young's modulus $E = 100.4$ GPa and Poisson's ratio $\nu = 0.2$ were given by Ma and Clarke [2]. The yield stress $\sigma_Y = 37.5$ MPa and power-law hardening exponent $n = 0.2$ are obtained by the fitting method of Section 3.3. It can be seen that the calculation results agree well with the test results at deep depth, but lower than the test results at the shallower depth.

The nominal indentation hardness H^* versus the indentation depth h for single crystal silver is shown in Figure 3a. Here $H^* = P/(24.56h^2)$, which is defined by Ma and Clarke [2]. From Figure 3a, one can see that the calculation results are much lower than the test results for shallower depth.

The calculation results on polycrystalline copper are shown in Figures 2b and 3b respectively, which have the same trends as Figures 2a and 3a.

Figure 4a shows the results of the indentation hardness H versus indentation depth h for single crystal silver. The indentation hardness H is defined as $H = P/\pi a^2$.

Since one cannot directly measure the contact area, the existed experimental data did not include any measured values of contact area. We only use the calculated values of the contact area instead the measured values of contact area. From Figure 4a,

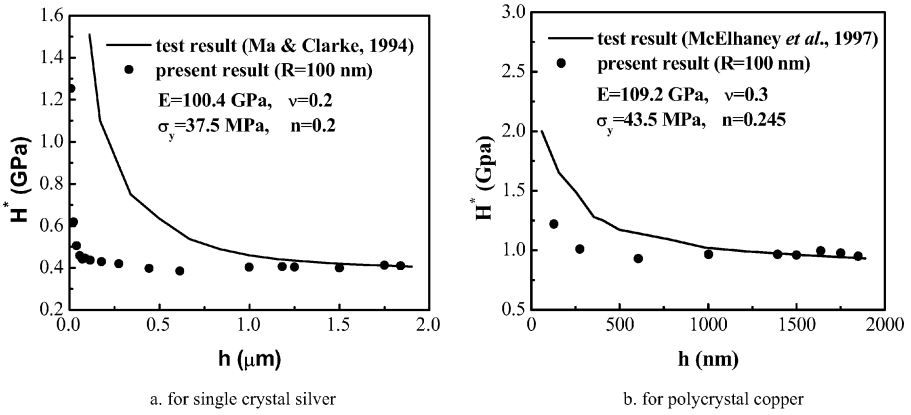

a. for single crystal silver b. for polycrystal copper

Fig. 3. The nominal indentation hardness H^* versus depth h, the calculation results are based on the classical J_2 plasticity theory.

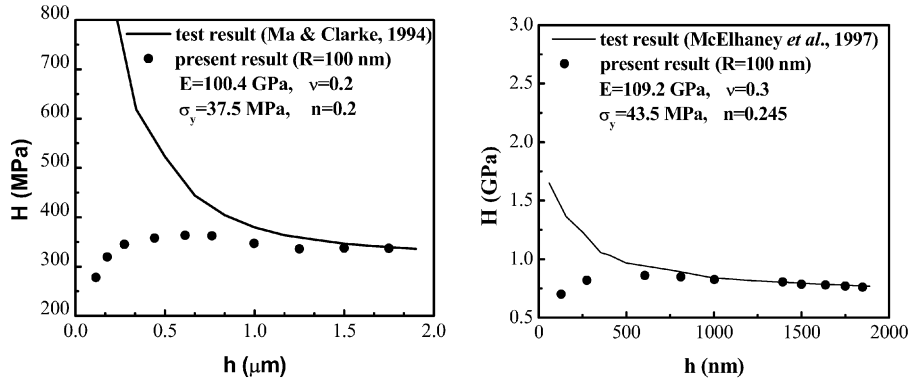

a. for single crystal silver b. for polycrystal copper

Fig. 4. The indentation hardness H versus depth h, the calculation results are based on the classical J_2 plasticity theory.

one can see that the calculation results are not only much lower than the test results, but the hardness decreases with the decreasing depth when the depth is lower than 500 nm. It means that the predicted load and hardness based on the conventional J_2 theory cannot agree well with the experimentally measured micro-indentation load and hardness over a wide range of the indentation depth, even considering the effect of indenter tip radius, which reveals that the indenter tip radius cannot explain the size effect.

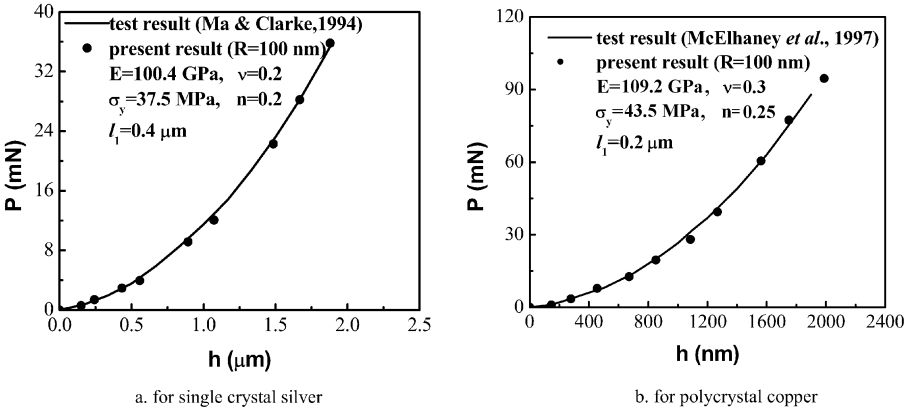

a. for single crystal silver

b. for polycrystal copper

Fig. 5. The indentation load P versus depth h, the calculation results are based on the strain gradient theory [7, 8].

4.2 Calculation Results for Strain Gradient Theory

The above results clearly show that the effect of the indenter tip radius cannot explain the size effect, so we carry out the calculations based on Chen and Wang's strain gradient theory [7, 8] with considering the influence of the indenter tip radius.

Figure 5a shows the results of the indentation load P versus indention depth h for single crystal silver. The solid line is the experimental results given by Ma and Clarke [2] and the full circles are the present calculation results. Young's modulus $E = 100.4$ GPa and Poisson's ratio $\nu = 0.2$ were given by Ma and Clarke [2]. The yield stress $\sigma_Y = 37.5$ MPa, power-law hardening exponent $n = 0.2$ and the intrinsic length scale $l_1 = 0.4$ μm are obtained by the fitting method of Section 3.3.

From Figure 5a, one can see that the predicted load agree very well with the experimentally measured micro-indentation load over the whole range of the indentation depth, which provides a validation of Chen and Wang's strain gradient theory [7, 8].

The nominal indentation hardness H^* versus the indention depth h for single crystal silver is shown in Figure 6a.

From Figure 6a, one can see that the predicted nominal indentation hardness agree very well with the experimentally measured nominal indentation hardness over the whole range of the indentation depth. Similar calculations are carried out on polycrystalline copper and shown in Figures 5b and 6b respectively, which have the same trends as Figure 5a and 6a.

5 Conclusions

The predicted load and hardness based on the conventional J_2 theory cannot agree well with the experimentally measured micro-indentation load and hardness at micron scales even considering the indenter tip radius, which means that indenter tip

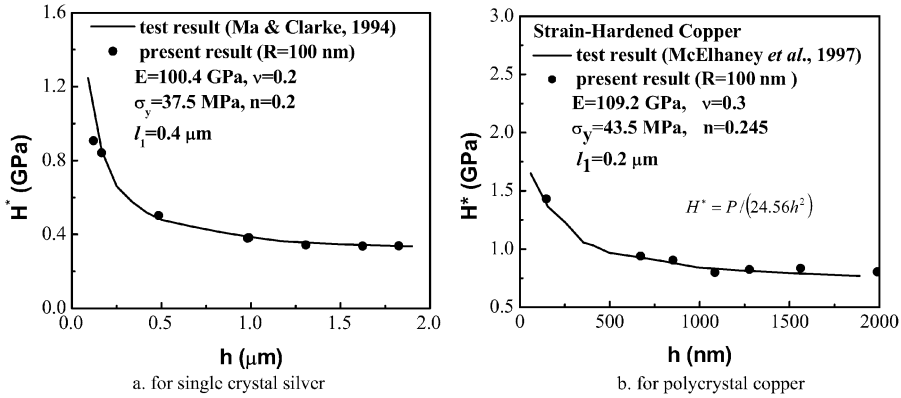

Fig. 6. The nominal indentation hardness H^* versus depth h, the calculation results are based on the strain gradient theory [7, 8]

radius is not the reason for size effect as some researchers said. While based on the strain gradient theory proposed by Chen and Wang [7, 8], the predicted load and hardness agree very well with the experimentally measured micro-indentation load and hardness over a whole range of the indentation depth.

Acknowledgments

This work is supported by the National Natural Science Foundation of China (10272103) and (10202023).

References

1. Stelmashenko, N.A., Walls, M.G., Brown, L.M. and Milman, Y.V., Microindentations on W and Mo oriented single crystals: An STM study, *Acta Metall. Mater.* **41**(10), 1993, 2855–2865.
2. Ma, Q. and Clarke, D.R., Size dependent hardness in silver single crystals, *J. Mater. Res.* **10**, 1995, 853.
3. McElhaney, K.W., Vlassak J.J. and Nix, W.D., Determination of indenter tip geometry and indentation contact area for depth-sensing indentation experiments, *J. Mater. Res.* **13**, 1998, 1300.
4. Fleck, N.A. and Hutchinson, J.W., Strain gradient plasticity. In J.W. Hutchinson and T.Y. Wu (eds.), *Advances in Applied Mechanics*, Vol. 33, Academic Press, New York, 1997, p. 295.
5. Gao, H., Huang, Y., Nix, W.D. and Hutchinson, J.W., Mechanism-based strain gradient plasticity – I: Theory, *J. Mech. Phys. Solids* **47**, 1999, 1239.
6. Huang, Y., Gao, H., Nix, W.D. and Hutchinson J.W., Mechanism-based strain gradient plasticity – II: Analysis, *J. Mech. Phys. Solids* **48**, 2000, 99.

7. Chen, S.H. and Wang, T.C., A new hardening law for strain gradient plasticity, *Acta Mater.* **48**, 2000, 3997–4005.
8. Chen, S.H. and Wang, T.C., A new deformation theory for strain gradient effects, *Int. J. Plasticity* **18**, 2002, 971–995.
9. Huang, Y., Xue, Z., Gao, H., Nix, W.D. and Xia, Z.C., A study of micro-indentation hardness tests by mechanism-based strain gradient plasticity, *J. Mater. Res.* **15**, 2000, 1786–1796.
10. Chen, S.H., Tao, C.J. and Wang, T.C., A study of micro-indentation with size effects, *Acta Mech.* **167**(1–2), 2004, 57.
11. Chen, S.H., Liu, L. and Wang, T.C., Strain gradient effects in nano-indentation of film-substrate systems, *Acta Mater.* **52**(5), 2004, 1089.
12. Li Min, Liang Naigang, Zhang Taihua, et al., 3D finite element simulation of the nanoindentation process, *Acta Mech. Sinica* **35**(3), 2003, 257 [in Chinese].
13. Swadener, J.G., George, E.P. and Pharr, G.M., The correlation of the indentation size effect measured with indenter of various shapes, *J. Mech. Phys. Solids* **50**, 2002, 681–694.
14. Dennis, Jr J.E. and More, J.J., Quasi-Newton methods – Motivation and theory, *SIAM Rev.* **19**, 1977, 46–89.